

Accepted Manuscript

Adhesion enhancement of DLC hard coatings by HiPIMS metal ion etching pretreatment



J.A. Santiago, I. Fernández-Martínez, A. Wennberg, J.M. Molina-Aldareguia, M. Castillo-Rodríguez, T.C. Rojas, J.C. Sánchez-López, M.U. González, J.M. García-Martín, H. Li, V. Bellido-González, M.A. Monclús, R. González-Arrabal

PII: S0257-8972(18)30467-5
DOI: doi:[10.1016/j.surfcoat.2018.04.090](https://doi.org/10.1016/j.surfcoat.2018.04.090)
Reference: SCT 23374
To appear in: *Surface & Coatings Technology*
Received date: 27 October 2017
Revised date: 17 April 2018
Accepted date: 30 April 2018

Please cite this article as: J.A. Santiago, I. Fernández-Martínez, A. Wennberg, J.M. Molina-Aldareguia, M. Castillo-Rodríguez, T.C. Rojas, J.C. Sánchez-López, M.U. González, J.M. García-Martín, H. Li, V. Bellido-González, M.A. Monclús, R. González-Arrabal, Adhesion enhancement of DLC hard coatings by HiPIMS metal ion etching pretreatment. The address for the corresponding author was captured as affiliation for all authors. Please check if appropriate. Sct(2017), doi:[10.1016/j.surfcoat.2018.04.090](https://doi.org/10.1016/j.surfcoat.2018.04.090)

This is a PDF file of an unedited manuscript that has been accepted for publication. As a service to our customers we are providing this early version of the manuscript. The manuscript will undergo copyediting, typesetting, and review of the resulting proof before it is published in its final form. Please note that during the production process errors may be discovered which could affect the content, and all legal disclaimers that apply to the journal pertain.

Adhesion enhancement of DLC hard coatings by HiPIMS metal ion etching pretreatment

J.A. Santiago^{a,f}, I. Fernández-Martínez^b, A. Wennberg^b, J.M. Molina-Aldareguia^a, M. Castillo-Rodríguez^a, T.C. Rojas^c, J.C. Sánchez-López^c, M. U. González^d, J.M. García-Martín^d, H. Li^e, V. Bellido-González^e, M.A. Monclús^a, R. González-Arrabal^f

a) IMDEA Materials Institute, c/Eric Kandel 2, 28906 Getafe, Madrid, Spain

b) Nano4Energy SL, José Gutiérrez Abascal 2, 28006 Madrid, Spain

c) Instituto de Ciencia de Materiales de Sevilla (CSIC-Universidad de Sevilla), Avda. Américo Vespucio 49, Isla de la Cartuja, 41092 Sevilla, Spain

d) IMN-Instituto de Micro y Nanotecnología (CNM-CSIC), 28760 Tres Cantos, Madrid, Spain

e) Gencoa Ltd, Physics Road, Speke, L24 9HP, UK

f) Instituto de Fusión Nuclear (UPM), José Gutiérrez Abascal 2, 28006 Madrid, Spain

Keywords: Adhesion, HiPIMS, Diamond-like Carbon (DLC), Hard coatings, Interface structure

Abstract

Poor adhesion is a recurrent problem for the wider use of diamond-like carbon (DLC) coatings in industrial applications. In this work, we investigate the effectiveness of high-power impulse magnetron sputtering (HiPIMS) metal ion etching to improve the adhesion of DLC coatings on high speed steel substrates. The influence of HiPIMS pretreatment parameters, the metal ion selection for the process and the addition of bonding layers on the adhesion properties were studied. Daimler-Benz and nanoscratch test methods were used to evaluate the adhesion. The elemental composition, morphology and microstructure of the samples were evaluated by EELS, SEM, AFM and HRTEM. In general, samples pretreated with HiPIMS metal ion etching withstand larger critical loads than those pretreated by conventional Ar^+ glow discharge and bonding layers. The pretreatment is proven to be very effective at removing surface contaminants and providing a gradual interface. The selection of Cr over Ti contributes to a significant improvement on the adhesion due to the reduction of the oxygen level at the interface thus ensuring an optimal coating-substrate contact and a more compliant structure, which prevents the delamination failure.

1. Introduction

Diamond-like carbon (DLC) coatings are widely used for tribological applications due to their outstanding properties, which include high hardness, low friction coefficient and excellent wear resistance [1-4]. The deposition of DLC coatings on engineering components is a standard activity in key industrial sectors including automotive [5, 6], micromachining [7], aeronautic [8] or biomedical [9]. The exceptional DLC tribomechanical properties are achieved by means of highly energetic deposition techniques such as cathodic arc evaporation (CAE), pulsed laser deposition (PLD), ion beam deposition, plasma immersion ion deposition, and magnetron sputtering (MS) [10-12]. As a result, typical DLC coatings are grown with high levels of compressive residual stresses, which limit the coating thickness, and usually lead to delamination failure [13, 14].

The lack of adhesion is a recurring problem not only for DLC but also for most of the coatings deposited using physical vapor deposition (PVD) processes [15]. In addition to high compressive residual stresses developed with highly energetic PVD techniques, the presence of contaminants at the substrate-coating interface, such as native substrate oxides, can also deteriorate adhesion, as it prevents the direct bonding between coating and substrate material. Native oxides and hydroxides promote weak metal-oxide bonding in comparison with metal-metal bonding, which decreases the interface strength. These negative effects are particularly evident when DLC is deposited onto steel substrates, and for this reason a number of techniques have been developed as pretreatment steps to improve DLC adhesion.

Traditionally, the substrate pretreatment is performed in an argon glow discharge plasma whereby contamination is sputtered away by bombardment with Ar^+ ions, which are accelerated towards the substrate with energies in the range of several hundred eV [16]. This method is easily implemented in industrial processes since argon is often used for subsequent sputtering deposition. However, there exist some limitations with this pretreatment, such as the low sputtering yield of carbon-based contaminants with Ar, the implantation of Ar^+ ions

into the substrate, which can occupy interstitial sites into the substrate lattice, thus inducing high elastic strain, and the diffusion and agglomeration of Ar species at the interface, which can lead to the formation of bubbles and a weaker interface [17, 18]. Improved adhesion values are achieved when the substrate pre-treatment is carried out with discharges that contain highly ionized metal fluxes, such as the ones achieved by cathodic arc or high power impulse magnetron sputtering (HiPIMS) [19].

HiPIMS is an emerging PVD technology characterized by very high power density pulses ($>1000 \text{ W/cm}^2$) at the sputtering target, which is typically two orders of magnitude larger than the average power density [18], with very short selectable pulse durations (50 – 200 μs) producing higher plasma densities than standard magnetron sputtering ($>10^{19} \text{ m}^3$). These features of HiPIMS meet the requirements of applications that are conventionally served by cathodic arc plasma processing such as substrate etching [20]. The metal ion etching with HiPIMS pretreatment was first reported by Ehiasarian *et al.* [21] for the pretreatment of substrates prior to nitride coatings deposition; the high content of metal ions in the bombarding flux boosted the etching of the substrate surface and facilitated the formation of a metal implanted area that promoted a strong bonding between the coating and the substrate. Different metal ion etching pretreatments with HiPIMS have been reported so far using Cr [22, 23], Nb [21], Al, Ti, W [24] and WC [25] for enhancing the adhesion of hard coatings such as CrN, TiAlN, CN_x or DLC. The selection of the metal for the etching pretreatment is usually done considering the chemical affinity of the coating-substrate system [24]. The chemical bonding strength together with the mechanical influence of the metal acting as a compliant interlayer reducing shear stresses, have been identified as main factors dictating the level of adhesion [26].

The aim of this study is to optimize the adhesion of DLC coatings deposited on high-speed steel (HSS) substrates using a HiPIMS metal ion etching pretreatment. The study focuses on the potential of HiPIMS to generate highly energetic Cr and Ti metallic ions that efficiently

remove oxides from the substrate surface and promote the formation of a gradual coating-substrate interface. The implantation elemental profiles into the substrate and the microstructure evolution across the interface were analyzed by Electron Energy-Loss Spectroscopy (EELS) and High-resolution Transmission Electron Microscopy (HRTEM) providing an atomic level insight into the interfacial structure and chemistry. Daimler-Benz and nanoscratch testing were performed to evaluate the adhesion enhancement obtained with the developed HiPIMS metal ion etching process.

2. Experimental methods

The deposition experiments were carried out in a custom-made batch type coating chamber designed by Nano4Energy S.L. with a volume of 0.8 m³ equipped with two rectangular graphite and WC:Co targets with an area of 400 cm² used for the deposition of the DLC and WC buffer layers respectively. A third 5 cm-diameter circular target was used for the metal ion pretreatment step with Cr or Ti. A sketch of the experimental setup is shown in Fig.1.

A hip-V 6 kW HiPIMS power supply with a peak power capability of 500 A at -1200 V was connected to the small circular magnetron to establish the Ti and Cr HIPIMS metal discharge. A second hip-V 6 kW power supply also able to operate up to -1200 V was used to apply the negative bias voltage to the substrate. An Enerpulse EN10 DC-Pulsed power supply was used for the deposition of the DLC and WC coatings. The argon working pressure was set to 0.65 Pa and the vacuum base pressure was kept under 10⁻⁴ Pa. Fig. 1 shows the substrate placement inside the chamber, at distances of 10 cm from the small circular magnetron for HiPIMS metal ion etching pretreatment and 13 cm from the WC and graphite targets during coating deposition.

Samples were deposited on square (20x20 mm²) mirror polished HSS substrates. The reason for choosing such small substrates was to ensure sample homogeneity along the whole size. Prior to any pretreatment, the substrates were cleaned using a sequence of ultrasonic washing with alkaline detergents, rinsing with de-ionized water, cleaning with isopropanol and air-

drying.

The parameters used for the different substrate pretreatment as well as for the deposition of the metal (Ti or Cr) bonding underlayer and DLC coatings are briefly described in the following:

1. Ar etching: an Ar^+ discharge was established at the substrates for 15 minutes, using a DC-pulsed bias voltage of -500 V and a frequency of 150 kHz.
2. HiPIMS metal ion etching: the substrates that underwent this step were biased to voltages in the range of -100 to -900 V. The target was operated in HiPIMS mode with the following parameters: pulsing time of 100 μs , repetition frequency of 100 Hz and pulsing voltages of 600 V (for Ti) and 1100 V (for Cr). The measured peak currents for Ti and Cr were 85 A and 22 A respectively. The etching time was set to 5 minutes for Ti and 15 minutes for Cr.
3. Deposition of Cr/Ti bonding underlayer: the magnetron was operated at the same conditions as in the previous step, but the substrate bias was reduced to -75 V. The time of this step was adjusted after a series of calibration steps (see more details in section 3.1.) to obtain a Cr/Ti bonding layer thickness between 5 to 10 nm.
4. Deposition of the WC interlayer: WC was deposited in DC-pulsed mode with a power density of 1.5 W/cm^2 , a peak voltage of 1050 V, a frequency rate of 150 kHz and a pulse width of 2.7 μs . The substrate was biased at -150 V. The thickness of this layer was approximately 100 nm.
5. Deposition of the DLC coating: DC-pulsed mode was used for DLC coatings deposition. The power density of the pulses reached values up to 3 W/cm^2 with a peak voltage of 1200 V at a repetition frequency of 150 kHz and a pulse width of 2.7 μs . A substrate voltage bias of -150 V was applied.

Seven samples were grown in order to study the effect of different deposition conditions on

the measured adhesion. The sample code and the processing steps that each particular sample underwent are depicted in Table 1.

For plasma characterization, voltage and current waveforms of the pulses applied on the target were measured using a high voltage differential probe (100:1 attenuation) and a PEM Rogowski probe sensor connected to a Tektronix TPS 2012 oscilloscope.

The topography of the plasma treated samples as well as the etching profiles were characterized by tapping mode AFM under ambient conditions using a Dimension Icon equipment from Bruker with super sharp probes (tip radius about 3 nm) by Bruker (model TESP-SS). Scanning electron microscopy (SEM) observations were performed using a FEI Verios 460 Field Emission XHR-SEM. High-resolution transmission electron microscopy and digital diffraction patterns (DDP) across the interface were obtained with an FEI Talos F200X TEM. Cross-sectional specimens for TEM analysis were produced by ion milling using a FEI Helios Nanolab 600i dual beam FIB-FEGSEM. For chemical distribution analysis, EELS spectra were recorded with a Gatan Imaging Filter (GIF, QUANTUM SE model) attached to a FEI Tecnai field emission gun scanning transmission electron microscope (STEM-FEG), mod. G2F30a with a high angle annular dark field (HAADF) detector from Fischione. The EELS spectra were measured in STEM mode using a probe with a size of less than 1 nm with a spectrometer collection angle of 19 mrad. The Gatan Digital Micrograph software was used for EELS spectra analysis.

Two methods were used to evaluate the adhesion strength. A first assessment was obtained following the Rockwell-C indentation test procedure described by the ISO26443:2008 [27]. An indentation load of 150 kgf is applied to the surface and the crater generated is examined by optical microscopy. The damage into the coating-substrate system is graded from HF1 to HF6 using the VDI guideline 3198 [28]. The grading provides qualitative assessment of the adhesion strength, the adhesion being adequate only for indents classified as HF 1 and HF 2. Secondly, scratch testing was used to quantitatively evaluate the adhesion strength of the DLC

coatings. Tests were performed with a Hysitron TI 950 triboindenter using a spheroconical diamond probe with an end radius of 10 μm . Progressive load nanoscratch tests (up to a normal force of 400 mN) were carried out while simultaneously recording lateral force and penetration depth. The nano-scratch test procedure involved three scans: one scratch pass at a loading rate of 10 mN/s, covering a length of 400 μm . A pre- and post-scan were also performed to evaluate the topography before and after the scratch. The critical load was determined from the sudden changes in the lateral force and depth data, which was completed with SEM observation to distinguish the failure modes. Five or more scratch tests separated by 100 μm were performed on each sample until reproducible results were obtained. The same triboindenter instrument equipped with a diamond Berkovich indenter was used to measure the DLC coating's hardness and reduced elastic modulus following the Oliver and Pharr method [29]. Reported values are an average of twenty indents performed using 2, 7 and 12 mN with loading, holding and unloading times of 5, 2 and 5 seconds respectively. The DLC coating residual stress was estimated using a substrate curvature method based on the Stoney equation [30]. Special samples were deposited on circular SS304 stainless steel substrates with a diameter of 25 mm and a thickness of 200 μm for this purpose. The radius of curvature of the surface was measured before and after film deposition with a Leica DCM3D optical profilometer.

3. Results and discussion

The DLC coatings of this study are classified as amorphous carbon (a-C), having a hardness of 29.4 ± 2.6 GPa and a reduced elastic modulus of 225 ± 17 GPa as measured by nanoindentation. The thickness of the films was ≈ 1 μm , having a compressive residual stress of ≈ 5 GPa. Further details on DLC coatings properties are described in [31].

3.1. Optimization of the HiPIMS metal ion etching pretreatment

HiPIMS is a deposition technology currently attracting much interest as new industrial applications emerge. Associated with its development, there is a need to establish correlations between the process parameters such as peak current, voltages or plasma duty cycles and the coatings growth mode. By varying the HiPIMS parameters it is possible to move from conditions of net deposition to metal ion etching, especially when working with highly ionized plasmas. In this case, the Ti and Cr HiPIMS discharges were operated at the highest peak current densities allowable in the low Ar pressure range, as it is well known that in HiPIMS operation mode, the ion-to-neutral ratio of the sputtered species is strongly dependent upon the peak current [32]. Very high peak current densities (up to 5 A/cm²) were achieved for Ti at a target voltage of 600 V (Fig. 2a). The bias current density collected at the substrate was 150 mA/cm² at a voltage bias of -450 V. As demonstrated in previous works [33], the occurrence of high peak current densities with the Ti target might be associated with the presence of multiply charged Ti ions (up to Ti⁺⁴) along with enhanced secondary electron emission. Therefore, only very low bias voltages might be necessary to perform efficient substrate metal etching. In the case of Cr (Fig. 2b), much lower current densities were obtained, reaching maximum values of 1 A/cm² at a target voltage of 1050 V with a bias current density of 30 mA/cm² measured when the substrate was biased at -750 V.

The transition from net deposition to substrate etching was measured for both Ti and Cr, as shown in Fig. 3. By using a masked stainless steel sample, the net deposition or substrate etching was evaluated as a function of substrate voltage. In the case of Ti, the substrate bias voltage threshold for ion etching is considerably lower (<400 V) than for Cr, where voltages over -750 V are required in order to reach etching conditions. This is largely due to the higher Ti ions charge state and ion-to-neutral ratio. It is well known that the kinetic energy of the ions generated during a plasma discharge and accelerated towards a negatively-biased

substrate is given by the charge states and the substrate voltage. As shown in the extended zone diagram [34], when the substrate bias voltage is increased, the sputtering yield in the substrate is enhanced and thus, the net deposition rate is reduced until effective ion etching is achieved. It is also worth mentioning that the high voltages and currents flowing to the substrate can cause undesirable arcing problems that can interrupt the normal operation of the power supplies. Therefore, proper arc management in both HiPIMS power supplies is required to achieve efficient metal etching results. In our case, this problem was solved by shutting down the voltage bias during an arc event in the magnetron to prevent etching inhomogeneities, and in the opposite case (during a substrate bias arc event) by extinguishing the plasma at the magnetron. Both power supplies were synchronized, particularly to prevent net deposition of metal during bias arc occurrence. Peak current control was carried out for arc detection in both the magnetron and substrate bias power supplies. Current limit values of 35 A for Cr, 100 A for Ti and 15 A for substrate bias were used.

The morphology and microstructure of the samples was characterized by TEM. Bright field cross-sectional TEM images shown in Fig. 4 demonstrate relevant differences when the HiPIMS pretreatment is applied in comparison to when it is not. Furthermore, significant changes are also observed when pretreatment is applied depending on the substrate bias voltage. The interface of DLC/WC sample without HiPIMS metal etching is shown in Fig. 4a. A low-density area is observed between the steel and the coating (marked by an arrow), which reveals the presence of impurities that have not been removed by Ar^+ etching only. The presence of these impurities leads to a poor contact between the coating and the substrate generating a weak adhesion spot. When increasing substrate voltage bias up to -600 V for Cr-HiPIMS pretreatment, the low-density area disappears and an amorphous layer with a thickness of 5 to 10 nm is observed on top of the substrate surface (Fig. 4b). The observation of similar amorphous layers when cleaning a substrate material with HiPIMS metal ions has

been previously reported [20]. It is worth noting that the extent of the amorphous layer coincides with the low-density area of impurities observed when no pretreatment is applied (Fig. 4a). TEM-EDX analysis reveals that oxygen and argon are still present within this amorphous layer but seem to be present at a much lower level. Over the Cr amorphous layer, a polycrystalline Cr layer is observed. The origin of the recrystallized Cr layer is still not clear. It may be due to a temperature enhancement at the layer surface related to the high ion bombardment flux, but more work needs to be done to clarify this issue.

Fig. 4c shows the morphology of a sample subjected to an Ar glow discharge plus a Cr-HiPIMS ion etching pretreatment at a bias voltage of -750 V (DLC/WC/Cr_{HiP}). Under these process conditions, the kinetic energy of Cr ions is sufficiently high to promote effective etching over net deposition. This situation leads to a clean interface with good coating-substrate contact. Fig. 4d shows the case when the etching rate is too high (almost -200 nm/h), as in the sample subjected to a Ti-HiPIMS ion etching at a voltage bias of -600 V. Titanium ions reach the substrate with a high kinetic energy that leads to a significant sputter removal of the steel substrate. The high arrival energy together with the high current flux obtained during the discharge produce a rough surface (rms roughness=17.4 nm). This situation is highly undesirable from the adhesion point of view as previously reported in Ref [35].

3.2. Adhesion tests

Fig. 5 shows typical results from the Daimler-Benz test for all the samples studied. In order to discuss the results we have divided the samples into two groups: (i) samples where HiPIMS pretreatment was not applied and (ii) samples that underwent an Ar glow discharge plus an additional HiPIMS metal-ion pretreatment. Regarding the first group (columns 1 and 2 of Fig. 5) we observe that the sample without any bonding layer (DLC/WC) exhibits an adhesion strength of HF6, which is inadmissible for industrial purposes. The addition of a Ti- or Cr-bonding underlayer improves the adhesion, avoiding spallation around the indent. However,

the strength quality of these samples depends on the metal selected for the bonding underlayer, being HF5 for the sample with Ti and HF1 for the sample with Cr. This difference in the strength quality is related to the extent of crack propagation, which is much larger in the sample containing Ti than in the one containing Cr.

By comparing the results obtained for both groups (see Fig. 5), it is clear that the addition of HiPIMS metal ion etching as a pretreatment step significantly contributes to enhance the adhesion. All the samples belonging to the second group show satisfactory adhesion, with a slight improvement in the Cr-HiPIMS pretreatment sample (HF1) over Ti-HiPIMS pretreatment sample (HF2). Moreover, adhesion is optimum (HF1) for both Cr and Ti, when the HiPIMS pretreatment is combined with a bonding underlayer.

Adhesion critical load values obtained from the scratch tests are consistent with the Daimler-Benz results, but provide more quantitative results. For coatings without any bonding underlayer and no HiPIMS pretreatment, the critical load values obtained are the lowest (80 mN). When a Ti underlayer was used, the adhesion strength is clearly improved, with critical load values reaching 150 mN. The same trend is observed when a Cr bonding layer was used, raising the critical load values from 80 to 240 mN. In order to decouple the effect of the HiPIMS pretreatment from the bonding underlayer, it is instructive to analyze the outcome of the scratch tests on the samples where the Cr- or Ti- HiPIMS ion etching pretreatments were employed without any bonding underlayers. For the titanium case, DLC/WC/Ti_{HiP} reaches a critical load of 194 mN whereas for chromium, DLC/WC/Cr_{HiP}, the value goes up to 310 mN. Therefore, the results show that the degree of adhesion improvement is larger when using only HiPIMS pretreatment than with the use of bonding layers only. Finally, the combination of both steps (HiPIMS ion etching pretreatment followed by a metallic bonding underlayer) produces the largest improvement in adhesion. These samples exhibit critical loads that reach 210 mN in the case of Ti and 380 mN in the case of Cr. This is reasonable, as both approaches can be considered complementary. On the one hand, the HiPIMS pretreatment efficiently

cleans the steel surface and provides an optimal coating-substrate contact ensuring the removal of amorphous layers that are usually developed under net deposition conditions, as shown in Fig. 4c. On the other hand, the addition of bonding layers enables the distribution of loads on larger interlayer areas relaxing stresses and reducing deformation [36, 37, 38]. Nevertheless, it is worth noting that the major difference in terms of adhesion is related to the metal that was selected for HiPIMS pretreatment. Critical load values are doubled when Cr ions are used instead of Ti ions. The adhesion strength difference is also reflected in the observation of different delamination modes.

Figs. 6a and 6b show optical micrographs and SEM images of the scratches as well as plots of normal force, lateral force and penetration displacement for the DLC/WC/Ti/Ti_{HiP} and DLC/WC/Cr/Cr_{HiP} respectively. When Ti pretreatment was used a brittle delamination mode is observed (Fig. 6a) with increased hemispherical (“kidney-shaped”) coating chipping failures extending over the side of the scratch track. The cracks formed along the track propagate a considerable distance before stopping in the form of a compressive spallation. Many of these cracks nucleate at large interfacial flaws such as polishing defects present in the substrate (Fig 6a). On the contrary, the delamination mode with Cr is ductile, as observed in Fig. 6b. A detailed view of the SEM image reveals a tensile buckling failure mode behind the indenter and sideward pile-up in the direction of the moving indenter. The pile-up of the material ahead and to the sides of the stylus causes the bending of the coating and controls the buckle failure mode [39], which places the coating surface in tension. The well-adherent and tough Cr underlayer forms strong bonds with the steel substrate and produces a more compliant coating-substrate system, which prevents the catastrophic adhesive failure. On the other hand, titanium undergoes a brittle failure because the compliance of the underlayer is not effective at minimizing shear stresses at the coating-substrate interface. These big differences in performance between Ti and Cr can be better understood in the light of the chemical and microstructural characterization of the interfaces, as shown below.

3.3. Elemental distribution, morphology and microstructure of coatings exhibiting enhanced adhesion

The elemental distribution, the morphology, and the microstructure of the DLC/WC/Ti/Ti_{HiP} and DLC/WC/Cr/Cr_{HiP} samples were investigated as a function of the distance from the substrate/coating in order to further elucidate the role of the selected metals for HiPIMS metal-ion pretreatments on the adhesion improvement.

Fig. 7a shows the elemental distribution of the DLC/WC/Ti/Ti_{HiP} sample as a function of the distance from the WC layer to the steel substrate characterized by EELS. The profile shows a region containing Ti of ≈ 6 nm of thickness underneath the WC layer followed by a region of ≈ 6 nm where Ti is implanted into the steel substrate (shaded area in Fig. 7a). These data are further corroborated by HRTEM image, see Fig. 7b. In this figure, we observe a layer with lower contrast corresponding to a Ti rich region. Ti ions have a high bonding affinity and are incorporated at lattice sites inside the steel substrate. It is worth mentioning that the oxygen signal showed in Fig. 7a follows the same trend than titanium, which is indicative of the formation of oxides due to the gettering effect of titanium [40, 41]. Gettering effect involves the formation of brittle oxide phases when the metal is saturated with gas [42]. The embrittlement of the titanium underlayer, due to the oxygen uptake, might not provide enough compliance to the structure and would lead to fracture, as observed in the scratch micrographs (Fig. 6a). The gettering of oxygen can take place from native oxide films present in the surface or by the diffusion of oxygen during the titanium deposition. The ratio Ti/O remains constant along the interface which points out to the dynamic diffusion of the oxygen during coating deposition as the main gettering factor. On that assumption, the amount of oxygen incorporated into the titanium layer is linked to the residual oxygen present within the chamber. Thus a careful control of vacuum base pressure is necessary to improve coating adhesion.

The elemental distribution of the DLC/WC/Cr/Cr_{HiP} is depicted in Fig. 7c. The Cr signal covers a wide range of ≈ 15 nm in depth. The first 8 nm correspond to the deposited Cr and the following ≈ 7 nm corresponds to Cr implanted in the substrate. The slight increase in the range of implantation for Cr ions is related with the higher voltage bias used for effective etching (-750 V) in comparison with that used for Ti (-450 V), which provides a higher energy of Cr ions. In contrast to the titanium case, the oxygen signal is negligible along the interface. As surface contamination species are kept at a very low level, metallic bonding is further promoted, which largely explains the adhesion enhancement of the Cr-ion etched samples.

In both cases a clean and dense interface is generated as a result of the intense bombardment and highly energetic incoming flux of metal ions with no visible bubbles, voids or droplets and a wide substrate-modified area (Figs. 7b and 7d) giving rise to a more gradual DLC-steel substrate interface.

A more detailed analysis of the microstructure along different regions of the substrate-coating interface was performed by HREM and DDP. For each region, the sample was tilted to the zone axis of one of the substrate grains. For DLC/WC/Ti/Ti_{HiP}, the HREM image of the interface in Fig. 8a shows a fully dense nanocrystalline Ti layer. The DDP in region 2 corresponds to the [111] zone axis of the underlying fcc steel grain, with a lattice parameter of $a_{\text{Fe}(\gamma)} = 3.59$ Å. The DDP in region 1 from the Ti underlayer suggests a heteroepitaxial growth of the Ti layer on the steel substrate, as evidenced by the coincident DDP's from the two regions. The fact that the Ti undertakes a substantial amount of oxygen, according to the EELS analysis, introduces an uncertainty on the determination of the crystal structure of this Ti underlayer. However, the nanocrystalline nature of the Ti layer is indicative of a moderate concentration of oxygen, as higher contents have been associated with the amorphization of titanium [41, 43]. Moreover, the heteroepitaxial growth indicates an intimate bonding with the

underlying substrate.

For DLC/WC/Cr/Cr_{HiP} specimens, the crystalline structure across the interface is shown in Fig. 8b. The Cr underlayer shows its equilibrium bcc crystal structure, with a lattice parameter of $a_{Cr} = 2.93$ (Å). The steel grain in this area was oriented in a [1 -1 -2] zone axis and the Cr grains in a [111] zone axis, but alignment of the diffraction patterns also suggests a heteroepitaxial relationship between them, with the {110} lattice planes of bcc Cr growing parallel to the {111} lattice planes of the fcc steel. A gradual transition from the fcc structure of the steel substrate to the bcc structure of the Cr underlayer was found as the Cr content increased across the interface, which reflects an intimate bonding between the substrate and the Cr layer.

Therefore, the HREM results show that the HiPIMS pretreatment alters considerably the interface structure, due to the highly energetic ion bombardment. For the case of Ti-ion etching pretreatment, a wide region of steel substrate is modified by the implantation of Ti ions and the Ti underlayers seems to grow heteroepitaxially, indicating a clean and free of contaminants interface. However, the Ti underlayer suffers a significant oxygen uptake, presumably from residual oxygen present within the chamber due to the getter effect of Ti. The steel region modified by Cr implantation is even wider, presumably due to the larger substrate bias during the Cr ion pretreatment. There is also evidence of some preferred orientation relationship of the Cr underlayer with the underlying steel substrate, again suggesting a clean and free of contaminants interface. Even though the development of an intimate bonding between the metallic underlayer and the substrate as a result of the HiPIMS pretreatment could suggest a very good adhesion strength [21] in both cases, the resulting DLC coating adhesion was much better for chromium than for titanium. The highly effective removal of oxides with Cr HiPIMS pretreatment appears to be a major factor for improving

adhesion because it promotes the formation of a metallic bonding layer with good adhesion that fails in a ductile mode. On the contrary, even though the Ti seems to be as effective on removing surface contaminants, oxygen uptake due to the getter effect of Ti during deposition results on a oxygen-rich Ti bonding layer, that can compromise the compliance of the interface. This assumption has been previously proposed when using titanium bonding layers [39] and agrees with the brittle deformation mode observed in the scratch tests.

4. Conclusions

The efficiency of Ti- and Cr- HiPIMS metal ion etching pretreatment as a tool for optimizing the DLC coating adhesion on steel substrates has been demonstrated. The HiPIMS pretreatment was carried out with Ti and Cr ions under different process conditions, which were successfully optimized to obtain fully dense substrate-coating interfaces without contaminants. All samples whose substrates underwent a HiPIMS metal ion etching pretreatment exhibited superior critical load values for coating failure in scratch testing compared with pretreatments performed with just argon glow discharges or intercalation of bonding layers.

The major reasons for the remarkable adhesion enhancement achieved by the HiPIMS pretreatment process are the effective removal of contamination and impurities such as native oxides and the ability to generate a gradual interface with metal ions. The adhesion of DLC coatings to the substrate is further improved when Cr is selected as the metal for pretreatment over Ti. This is due to the higher capability of Cr to remove oxides from the interface which facilitates the metal bonding with the steel substrate. Moreover, a more compliant interface was obtained when Cr-HiPIMS pretreatment was used, which improves the stress distribution and reduces the coating deformation under load. The exceptionally high critical load values presented here are of great interest for the industrial-scale deposition of DLC hard coatings.

Acknowledgments

The research leading to these results has received funding from Madrid region under programme S2013/MIT-2775, DIMMAT project. Financial support from MINECO under projects (RADIAFUS IV ENE2015-70300-C3-3-R, MAT2014-59772-C2-1-P, MAT2015-69035-REDC FUNCOAT+), Leverhulme International Network Grant (CARBTRIB) and EUROfusion Consortium under project AWP15-ENR-01/CEA-02 are also acknowledged, as well as the service from the X-SEM Laboratory at IMN under project CSIC13-4E-1794 with support from EU (FEDER, FSE).

ACCEPTED MANUSCRIPT

References

- [1] Tribology of Diamond-Like Carbon films: Fundamentals and Applications, Springer, N. York, 2007
- [2] J. Robertson, Surface and Coatings Technology 50 (1992) 185-203
- [3] A. Grill, Diamond and Related Materials 8 (1999) 428-434
- [4] K. Bewilogua, D. Hofmann, Surface and Coatings Technology 242 (2014) 214-225
- [5] K.A.H. Al Mahmud, M. Varman, M.A. Kalam, H.H. Masjuki, H.M. Mobarak, N.W.M. Zulkifli, Surface and Coatings Technology 245 (2014) 133-147
- [6] A. Erdemir, C. Donnet, J. Phys. D: Appl. Phys. 39 (2006) 311-327
- [7] S. Bhowmick, A. T. Alpas, International Journal of Machine Tools and Manufacture 48 (2008) 1429-1443
- [8] K. Miyoshi, Wear 251 (2001) 1061–1067
- [9] R. Hauert, Diamond and Related Materials 12 (2003) 583-589
- [10] J. Robertson, Materials Science and Engineering: R: Reports, 37 (2002) 129-281
- [11] A. Anders, Some applications of cathodic arc coatings, Springer, N. York, 2008, 1-62
- [12] J. Robertson, Diamond and Related Materials, 2 (1993) 984-989

- [13] K. Bobzin, T. Brögelmann, C. Kalscheuer, M. Engels, *Surface and Coatings Technology* 308 (2016) 80-89
- [14] Y. Lin, A.W. Zia, Z. Zhou, P.W. Shum, K.Y. Li, *Surface and Coatings Technology* 320 (2017) 7-12
- [15] H. Oettel, R. Wiedemann, *Surface and Coatings Technology* 76-77 (1995) 265-273
- [16] M. Ohring, *The materials Science of Thin Films*, Academic Press, N. York, 1992, p.129
- [17] J.C. Bean, G.E. Becker, P.M. Petroff, T.E. Seidel, *J. Appl. Phys.* 48 (1977) 907
- [18] J.W. Mayer, L. Eriksson, J.A. Davies, *Ion Implantation in Semiconductors*, New York, 1970
- [18] A. Anders, *Surface and Coatings Technology* 200 (2005) 1893
- [19] K. Sarakinos, J. Alami, S. Konstantinidis, *Surface and Coatings Technology* 204 (2010) 1661-1684
- [20] A. Anders, *Surface and Coatings Technology* 257 (2014) 308-325
- [21] A.P. Ehiasarian, J.G. Wen, I. Petrov, *J. Appl. Phys.* 101 (2007) 054301
- [22] E. Broitman, Zs. Czigany, G. Grecynski, J. Bohlmark, R. Cremer, L. Hultman, *Surface and Coatings Technology* 204 (2010) 3349-3357
- [23] M. Latterman, A.P. Ehiasarian, J. Bohlmark, P.A.O. Persoon, U. Helmersson, *Surface*

and Coatings Technology 200 (2006) 6495-6499

[24] K. Bakoglidis, S. Schmidt, G. Greczynski, L. Hultamn, Surface and Coatings Technology 302 (2016) 454-462

[25] WD. Munz, M. Schenkel, S. Kunkel, J. Paulitsch, K. Bewilogua, J. Phys: Conf. Ser. 100 (2008) 082001

[26] D. Galvan, Y.T. Pei, J.Th.M. De Hosson, Acta Materialia 53 (2005) 3925-3934

[27] ISO 26443:2008. Fine ceramics (advanced ceramics, advanced technical ceramics). Rockwell indentation test for evaluation of adhesion of ceramic coatings

[28] Verein-Deutscher-Ingenieure, Daimler-Benz Adhesion Test, VDI 3198, VDI-Verlag, Dusseldorf, 1992, p.7

[29] W.C. Oliver and G.M. Pharr, J. Mat. Res., 7, 1564-1582 (1992)

[30] CEN/TS 1071-11:2005: Advanced technical ceramics: Methods of test for ceramic coatings, Part 11: Determination of internal stress by the Stoney formula

[31] I. Fernández-Martínez, J.A. Santiago, Bellido-González, V. et al., Society of Vacuum Coaters 59th Annual Technical Conference Proceedings, 126-131 (2016)

[32] A. Anders, Appl. Phys. Lett. 92 (2008) 201501

[33] J. Andersson, A.P. Ehasarian, A. Anders, Appl. Phys. Lett. 93 (2008) 071504

[34] A. Anders, Thin Solid Films 518 (2010) 4087-4090

[35] J. Takadoum, H. Houmid Bennani, Surface and Coatings Technology 96 (1997) 272-282

[36] A. Grill, B. Meyerson, V. Patel, Journal of Materials Research 3 (1988) 214-217

[37] H. Ronkainen, J. Vihersalo, S. Varjus, R. Ziiacus, U. Ehrnsten, P. Nenonen, Surface and Coatings Technology 90 (1997) 190-196

[38] C. Dumkum, D.M. Grant, I.R. McColl, *Diamond and Related Materials* 6 (1997) 802-806

[39] S.J. Bull, *Surface and Coatings Technology* 50 (1991) 25-32

[40] S.J. Bull, P.R. Chalker, C.F. Ayres, D.S. Rickerby, *Materials Science and Engineering: A*, 139 (1991) 71-78

[41] K.A. Pischow, L. Eriksson, E. Harju, A.S. Korhonen, *Surface and Coatings Technology* 58 (1993) 163-172

[42] V.L. Stout, M.D. Gibbons, *J. Appl. Phys.* 26 (1955) 1488

[43] N. Martin, C. Rousselot, D. Rondot, F. Palmino, R. Mercier, *Thin Solid Films* 300 (1997) 113-121

ACCEPTED MANUSCRIPT

List of tables

Table 1. Schematic representation of the steps performed for the deposition of the studied samples

Tables

<i>Sample code</i>	<u><i>Ar etching</i></u>	<u><i>Ti etching</i></u>	<u><i>Ti layer</i></u>	<u><i>Cr etching</i></u>	<u><i>Cr layer</i></u>	<u><i>WC layer</i></u>	<u><i>DLC coating</i></u>
DLC/WC	X					X	X
DLC/WC/Ti_{HIP}	X	X				X	X
DLC/WC/Ti	X		X			X	X
DLC/WC/Ti/Ti_{HIP}	X	X	X			X	X
DLC/WC/Cr_{HIP}	X			X		X	X
DLC/WC/Cr	X				X	X	X
DLC/WC/Cr/Cr_{HIP}	X			X	X	X	X

Table 1

List of Fig. captions

Fig. 1. Schematic configuration of the sputtering chamber.

Fig. 2. a) Current (top) and voltage (bottom) waveform for a Ti plasma discharge during the HiPIMS metal ion etching pretreatment. b) Current (top) and voltage (bottom) waveform for a Cr plasma discharge during the HiPIMS metal ion etching pretreatment.

Fig. 3. Deposition and etching rates evaluated for Cr and Ti HiPIMS pretreatment under different applied substrate bias voltages. A transition from net deposition to etching is observed in both cases. Conditions b, c and d were analyzed with cross-sectional TEM micrographs in Fig.2.

Fig. 4. Cross-sectional TEM images showing different coating-substrate interfaces: a) Observation of a low-density interface area for the DLC/WC sample without HiPIMS metal etching, between WC coating and HSS substrate. b) Amorphous transition layer for a Cr-HiPIMS pretreatment with -600 V substrate bias voltage under net deposition conditions. c) Clean interface with optimal coating-substrate contact observed for a sample whose substrate was pretreated with Cr-HiPIMS and biased at -750 V. d) Top-view SEM image showing the roughness induced on steel substrate surface for a sample whose substrate was pretreated with Ti-HiPIMS and biased at -600V.

Fig. 5. Optical micrographs of the Rockwell indents for the different specimens of the study. The adhesion strength HF as well as the critical load values are shown in each case.

Fig. 6. Nanoscratch test results for DLC/WC/Ti/Ti_{HiP} and DLC/WC/Cr/Cr_{HiP} samples. Evolution of the normal force (blue), lateral force (red) and depth displacement (green) with the lateral displacement. Optical micrographs of the scratch tracks and SEM images of the failure mode for titanium (left) and chromium (right).

Fig. 7. Line-scans EELS elemental distribution analysis of the (a) Ti-HiPIMS and (c) Cr-

HiPIMS pretreated interfaces and cross-sectional HRTEM images of the (b) DLC/WC/Ti/Ti-implanted/HSS steel and (d) DLC/WC/Cr/Cr-implanted/HSS steel interfaces.

Fig. 8. a) Cross-sectional HRTEM images of HSS steel substrate and the subsequent titanium underlayer (bright contrast) (left). Digital diffraction patterns (DDP's) obtained from HSS steel substrate region (bottom-right) and for the Ti underlayer region (top-right) b) Cross-sectional HRTEM images of HSS steel substrate and the subsequent chromium underlayer region (bright contrast) (left). DDP's obtained from HSS steel substrate (bottom-right) and for the Cr layer region (top-right).

ACCEPTED MANUSCRIPT

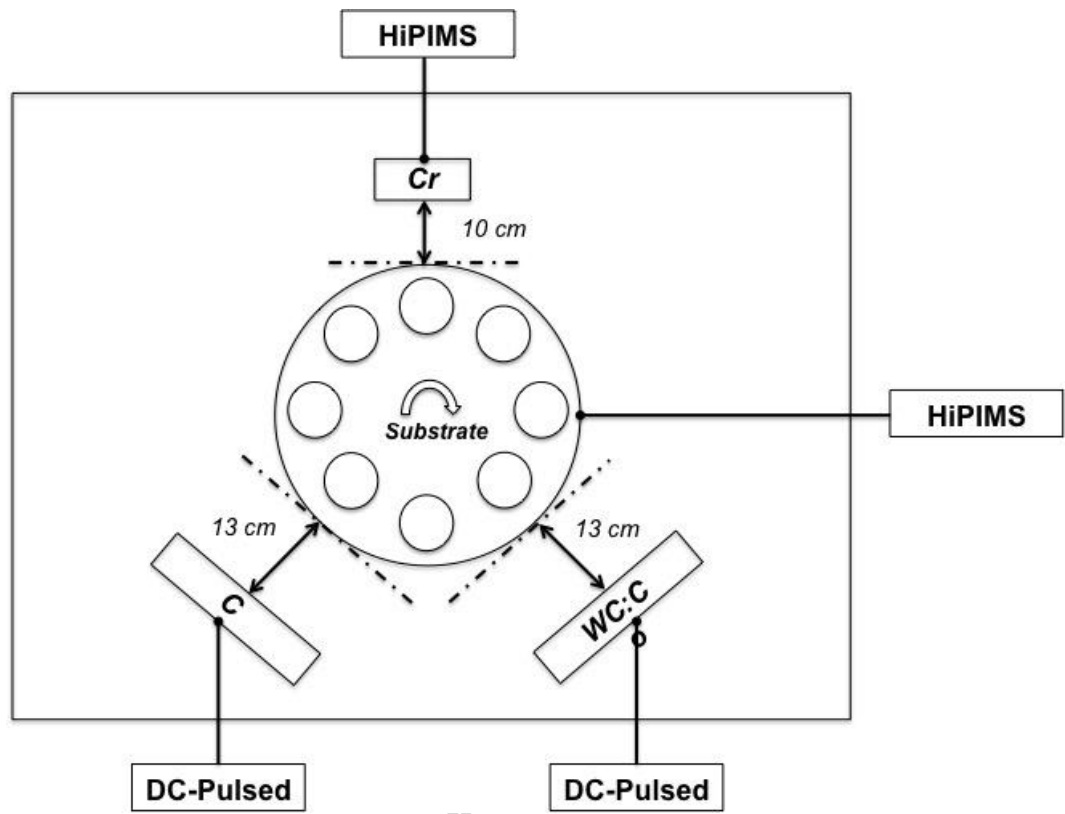


Fig. 1

ACCEPTED MANUSCRIPT

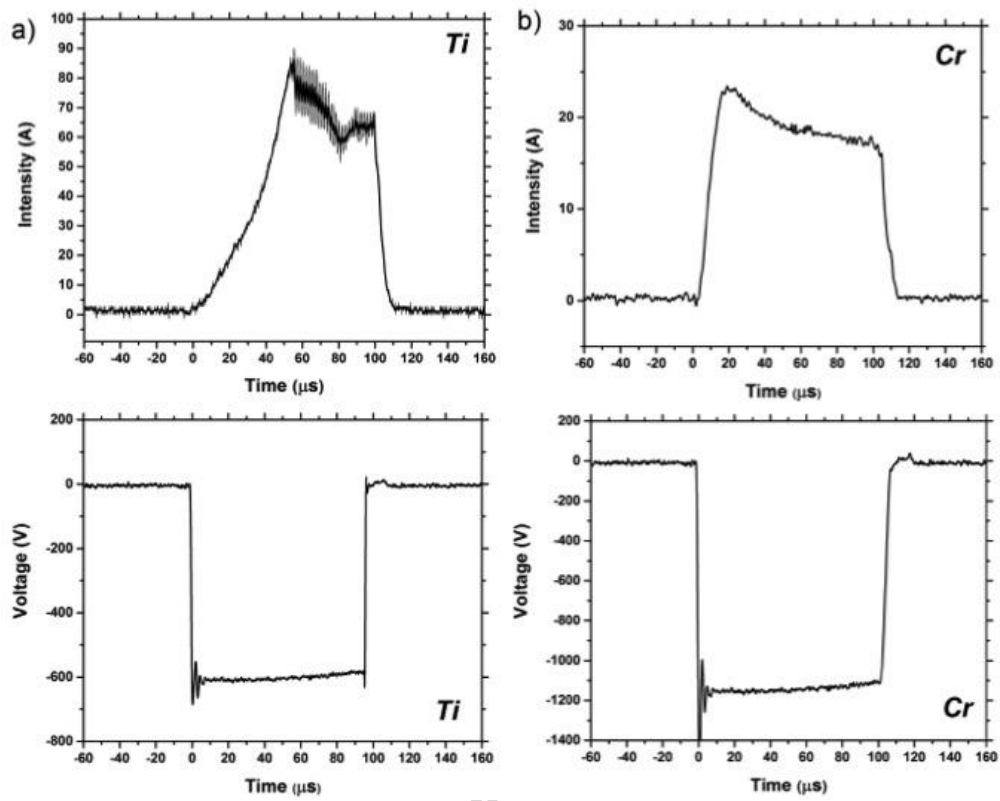


Fig. 2

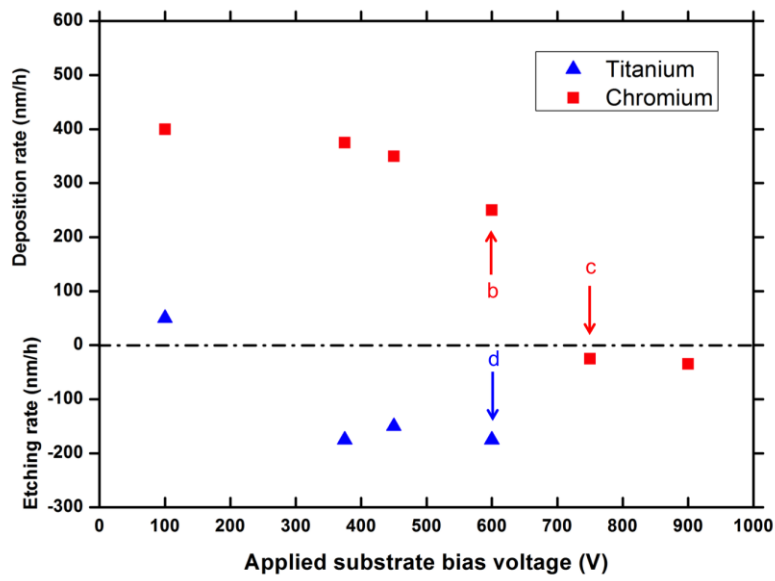


Fig. 3

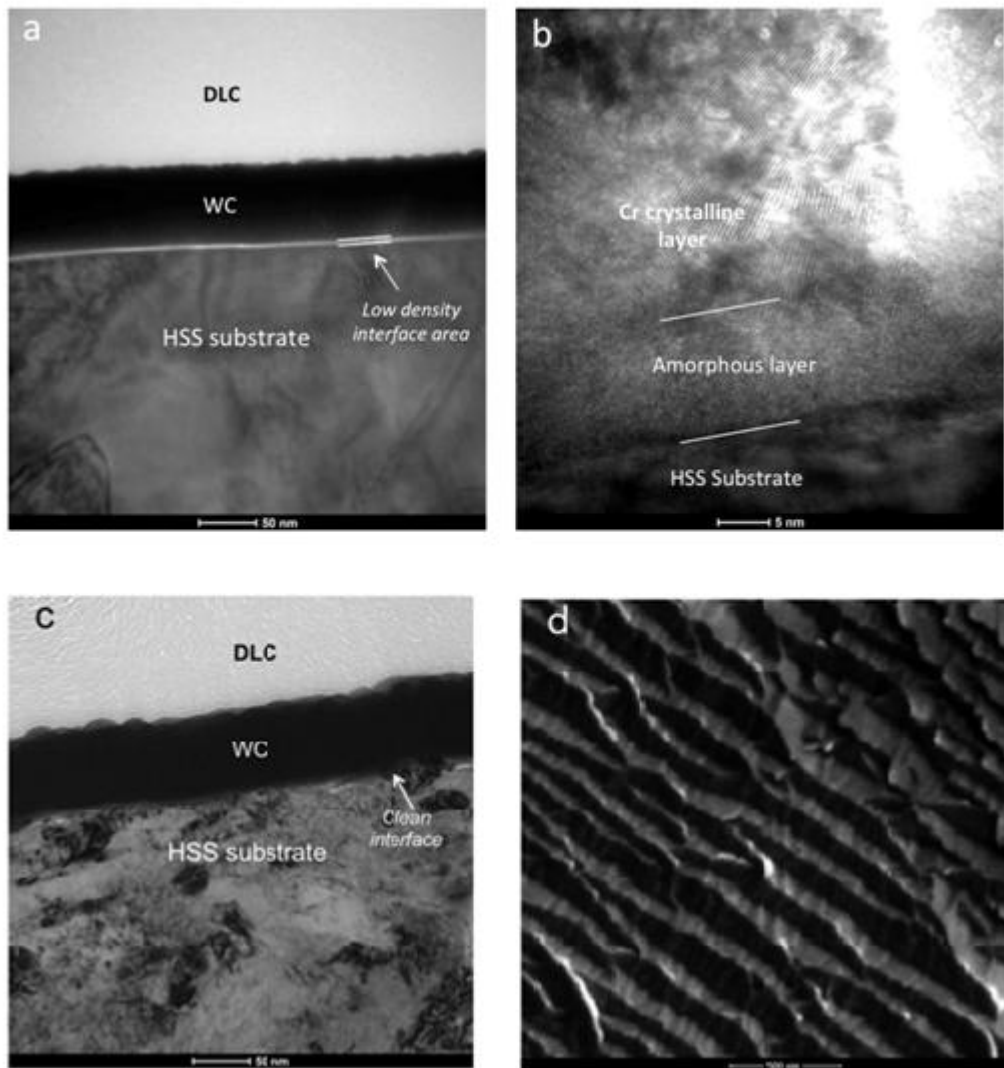


Fig. 4

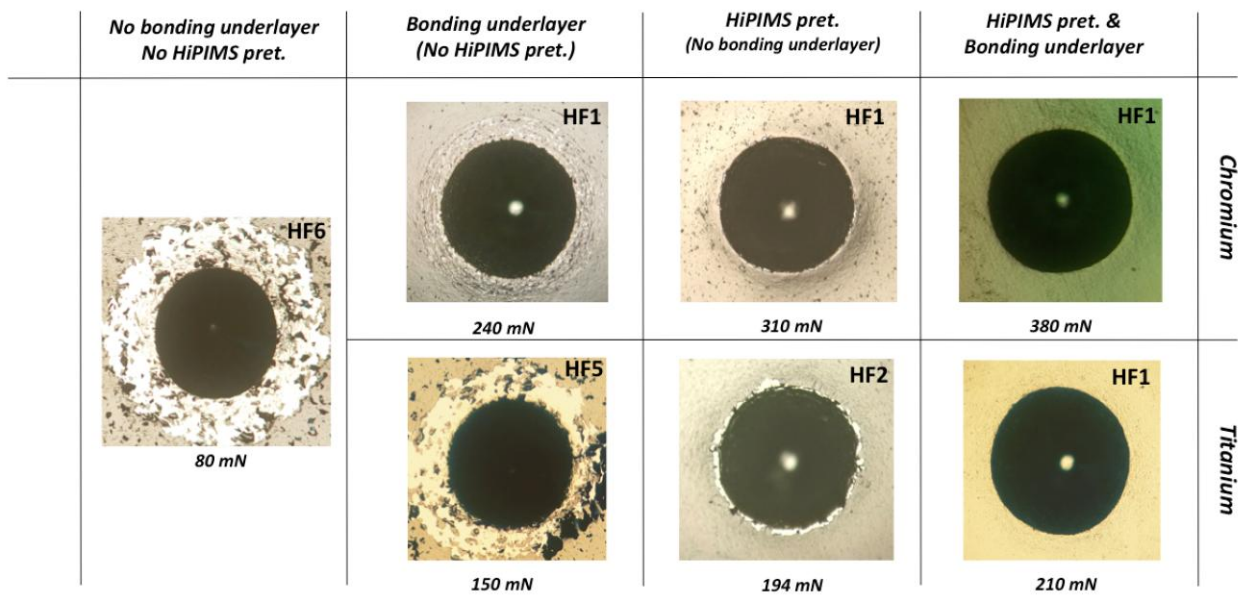


Fig. 5

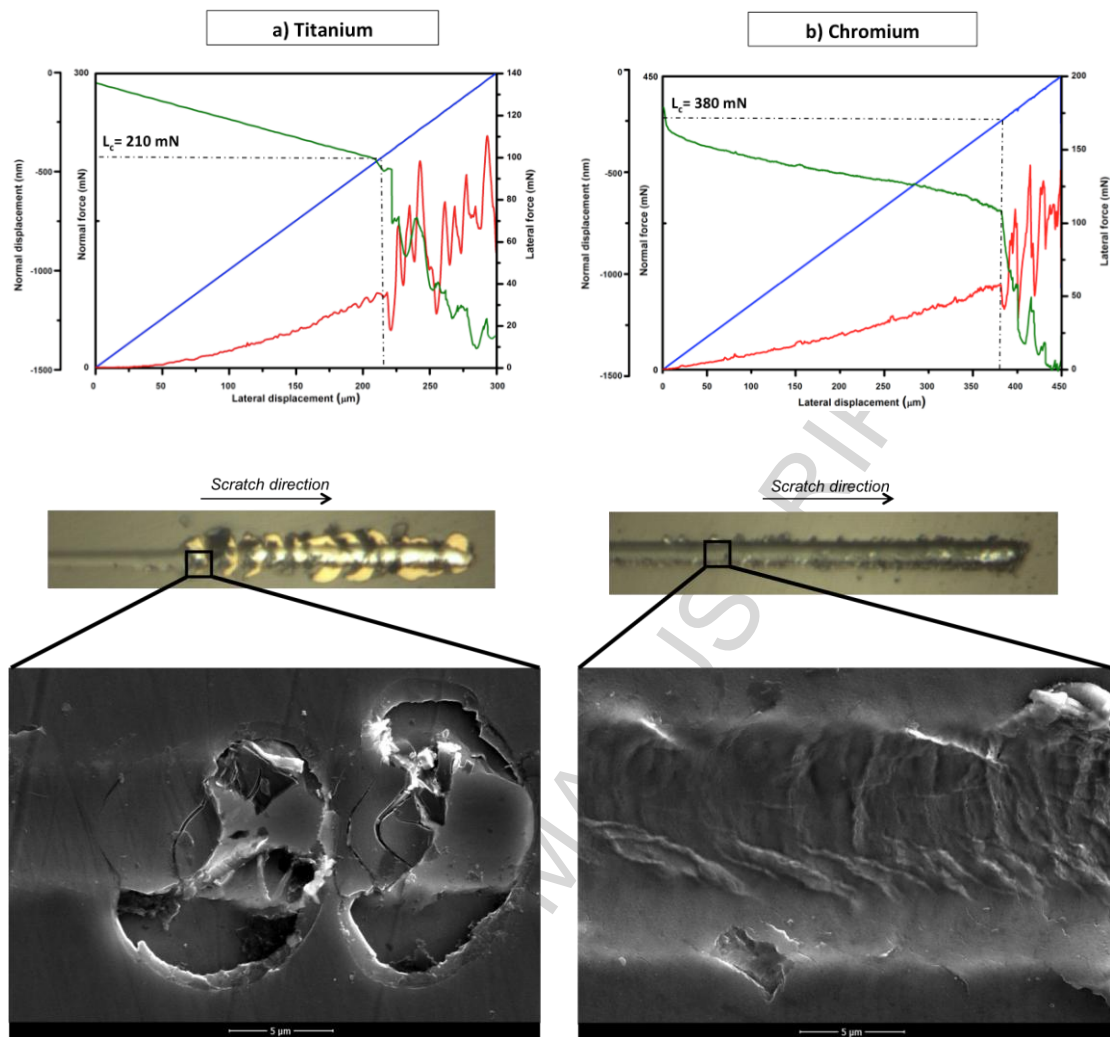


Fig. 6

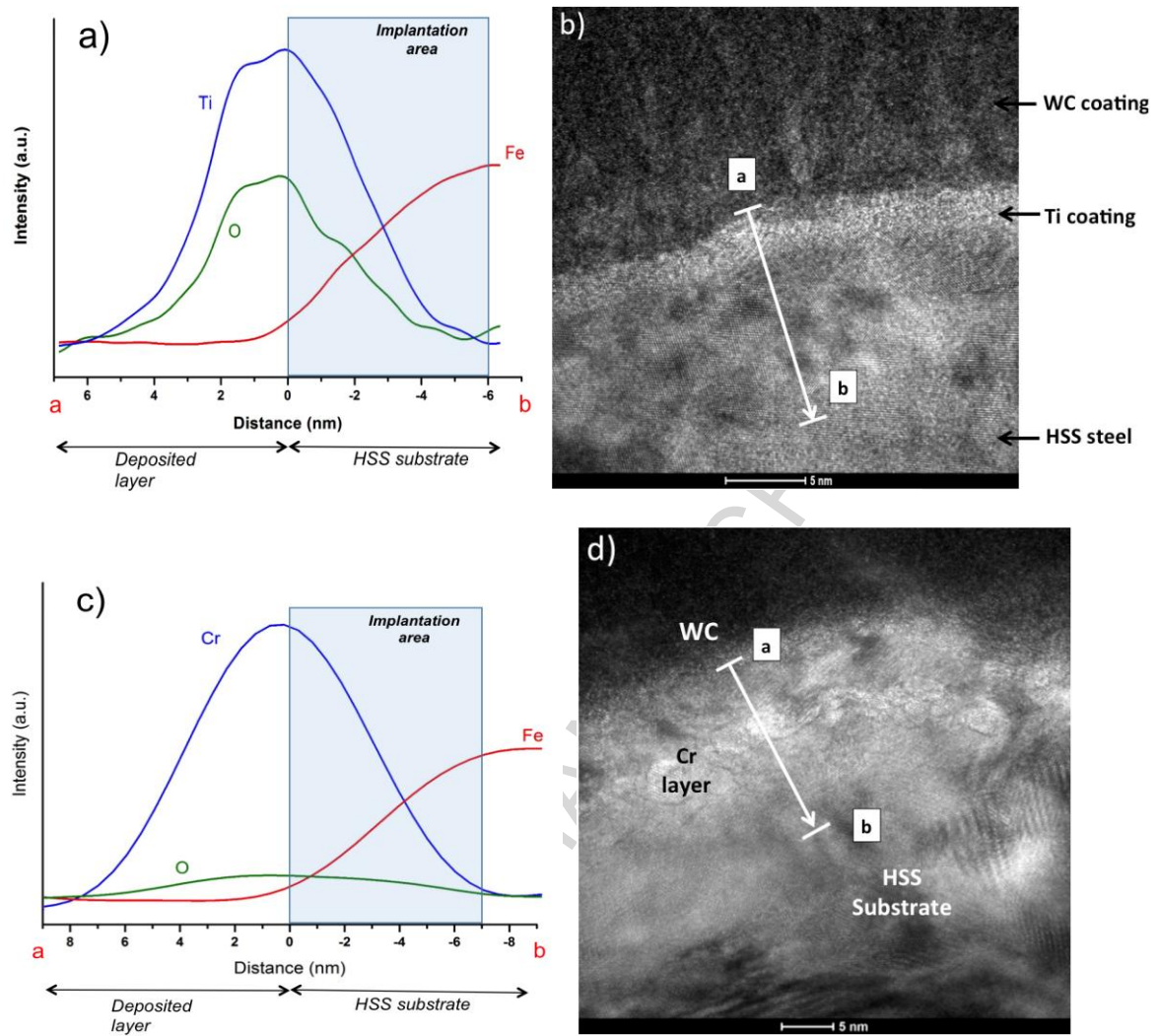


Fig. 7

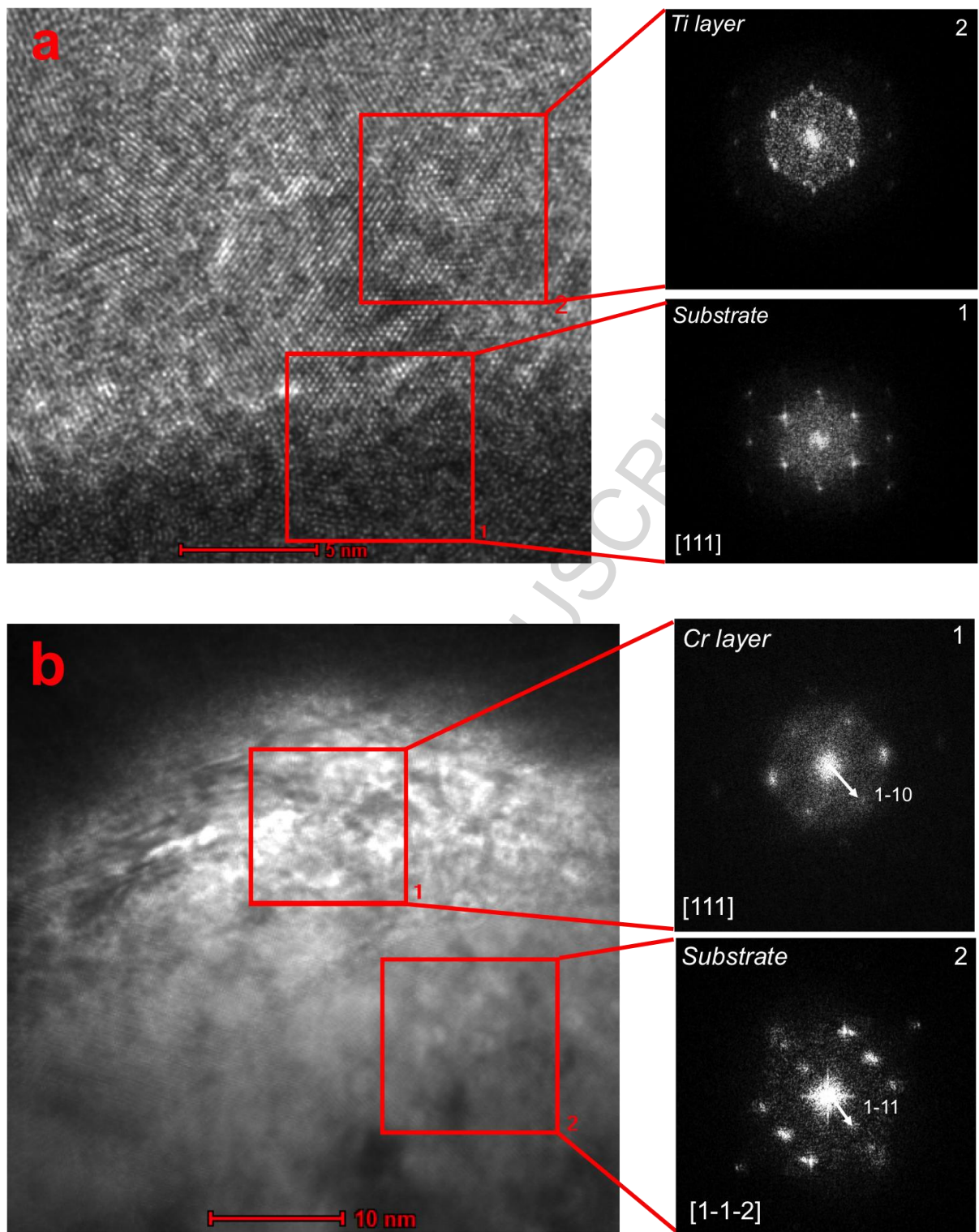


Fig. 8

Adhesion enhancement of DLC hard coatings by HiPIMS metal ion etching pretreatment

Highlights:

- HiPIMS pretreatment method for enhanced DLC adhesion on steel substrates is proposed.
- HiPIMS metal ion etching process parameters are optimized for Cr and Ti.
- Improved adhesion relates to substrate oxides removal and a gradual interface.
- Superior DLC adhesion with Cr due to lower O₂ gettering and more compliant interface.

ACCEPTED MANUSCRIPT